Influence of Axial Loads to Propagation Characteristics of the Elastic Wave in a Non-Uniform Shaft

Yimin Wei*, Zhiwei Zhao, Wenhua Chen and Qi Liu

Abstract

The vibration propagates through the shaft in the form of elastic waves. The propagation characteristics of the elastic waves are affected by the axial loads. The influence of the axial loads to the propagation characteristics of the elastic waves is studied in this paper. Firstly, the transfer matrix of the elastic waves for the non-uniform shaft with axial loads is deduced by combining the transfer matrix without axial load and the additional equation caused by the axial load. And then, a numerical method is used to study the influence of the axial load, non-uniformity and the rotating speed to the propagation characteristics of the elastic waves. It's found that a new Stop Band will appear due to the axial force, and the central frequency of which will decrease as the increase of the force, while the band width of which remains the same. The central frequency of the new Stop Band will also increase as the increase of the cross-section area ratio; however, the rotating speed of the shaft doesn't affect the propagation characteristics of the elastic waves obviously. Finally, an experimental rig is built up for further study, even though there are some small local errors, the results of experiments match well with the numerical ones, which indicates the validation of the theoretical results. The result can help to study the influence of the axial load to the dynamics of a non-uniform shaft and help to reveal the vibration propagating mechanism in such a shaft.

Keywords: Axial force, Propagation characteristic, Non-uniform shaft, Elastic wave, Transfer matrix

1 Introduction

The rotating shaft often suffers axial loads in real applications and the loads increase gradually as the unstop development of the machinery, e.g., the shaft of a large compressor, the rotor of a heat pump system, the dynamics of the rotating shaft with axial loads have drawn people's attention [1–3]. Besides the axial load, the rotating shaft are often non-uniform, e.g., with non-uniform cross-section, with variable elastic modulus [4–6]. These factors have a non-negligible influence on the vibration propagating in the shaft. Vibration propagates in the media such as a shaft in the form of elastic waves, the study to the propagation characteristics of the elastic wave can help to know the dynamics of the rotating shaft,

and also can help to control the unnecessary vibration, to reduce the noise, even to detect a crack [7–9].

The research to axial loads on a rotating shaft never stops. Kocakaplan et al. [10] studied the incremental wave motion in elastic media with initial stress, and how the initial stress produces changes in stiffness and wave propagation speeds was investigated. Ahmadi and Mahvelati [11] presented a new and simple approach for estimating group efficiency of drilled shafts installed in sandy soil under axial loading. Eftekhari et al. [12] investigated the nonlinear vibration of a simply supported rotating shaft with nonlinear curvature and gyroscopic effect under transversely electromagnetic load. Huang et al. [13] presented a method for assessing the dynamic stability of simply supported columns with damping under arbitrary periodic axial loading owing to parametric resonance. Chen et al. [14] performed experiments to investigate the interaction between bending moment and axial load for grouted connection specimen. Dai et al.

*Correspondence: yiminwei@126.com
National and Local Joint Engineering Research Center of Reliability
Analysis and Testing for Mechanical and Electrical Products, Zhejiang Sci-
Tech University, Hangzhou 310018, China

Wei *et al. Chin. J. Mech. Eng.*   (2019) 32:70

Page 2 of 13

[15] analyzed the parametric stability of rotating cylindrical shells under static and time dependent periodic axial loads. Gholipour et al. [16] evaluated the effects of axial load on dynamic responses and failure behaviors of reinforced concrete columns subjected to lateral impact loading by using numerical simulations in LS–DYNA. Johansen et al. [17] studied the offshore jacket structures carrying variable axial loads, large shear forces and bending moments. Dong et al. [18] presented an analytical study that predicts the low-velocity impact response of a spinning functionally graded graphene reinforced cylindrical shell subjected to impact, external axial and thermal loads. Yang et al. [1] built an experimental rotor rig and studied the axial load and rub, a comparison about the dynamic characteristics of the experimental rig is made between with and without the axial loads.

As for the studies about the propagation characteristics of the elastic wave, more concerns focused on the Pass and Stop Bands of the elastic waves [19, 20]. Fabro et al. [21] investigated the structural wave propagation in one dimensional waveguides with randomly varying properties along the axis of propagation. Li [22, 23] reduced the governing differential equations for free longitudinal vibration of rods with variable cross-section to the Bessel forms or other analytically solvable differential ones. Toso [20] analyzed the propagation characteristic including the cut-off frequency, Pass and Stop Bands of the longitudinal wave propagating in stepped rods or shafts, and the equations of wave motion of the element on the rod or the shaft were employed to deduce the transfer matrix and relationship between the propagation characteristic and the material properties and variation forms of the cross-section area. Abarbanel et al. [24] investigated linear wave propagation in non-uniform medium under the influence of gravity. Bahrami et al. [25] presented the wave propagation approach for analyzing the free vibration and wave reflection in carbon nanotubes. Xie et al. [26] presented a unified analytic method, wave based method to investigate free and forced vibrations of non-uniformly supported cylindrical shells. Tavasoli et al. [27] concluded that the application of non-uniform cross section piles increase the driving process efficiency, reduce energy consumption and decrease the noise pollution. Xue et al. [28] used Hermitian wavelet finite element can be used to describe the wave propagation and to reveal the rule of the wave propagation in plane. The wave propagation response is used to solve the load identification inverse problem. Sarayi et al. [29] employed wave propagation method to exactly derive resonant frequencies and wave power reflection from different classical boundary conditions. Bahrami et al. [30] presented the wave propagation approach for free vibration analysis of non-uniform annular and circular membranes.

Nevertheless, an important question of interest, which to our knowledge have not been addressed in most previous studies, is the influence of axial loads to the dynamics of the rotating shaft and to the propagation characteristics of the elastic waves, which need to be studied further.

Recently, the authors have studied the propagation characteristics of the elastic waves propagating in a rod, and in a multi-step rod by adopting the transfer matrix method, see references [5, 6], the rod or the multi-step rod is stationary, and further, the propagation characteristics of the elastic waves propagating in a non-uniform shaft is studied with considering the rotating speed, see Ref. [31]. In this study, the axial load of the non-uniform rotating shaft is considered, the influences of the axial load, the area-ratio and the rotating speed to the propagation characteristics of the elastic wave are studied.

The transfer matrix method is applied to study the influence of the axial loads to the elastic waves in this paper. First, the additional equation for the axial loads to the transfer matrix is deferred, and by combing it with the transfer matrix without axial loads, the whole transfer matrix is deduced for the non-uniform rotating shaft suffering axial loads. Then, the theoretical results are derived by using the numerical method, the influences of the axial load, the area-ratio and the rotating speed are studied thoroughly. Finally, an experimental rig is built up to verify the results of the theoretical study.

2 Theoretical Study
2.1 Propagation Characteristics
A non-uniform shaft is shown in Figure 1. As can be seen in the figure that the cross-section area varies as the location x. E is the elastic modulus of the material of the shaft, $S(x)$ is the cross-section area of the shaft at location x, ρ is the density, γ is the Poisson's ratio and L is the length of the shaft.

Usually, the motion status of an element on the shaft can be expressed by a state vector
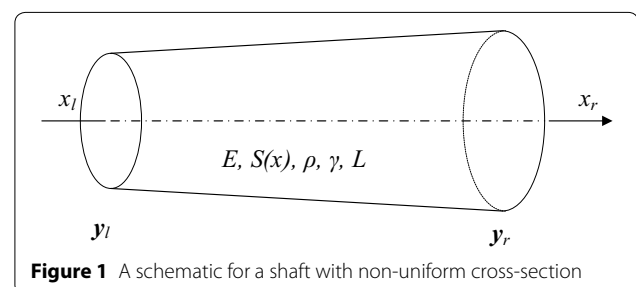
Figure 1 A schematic for a shaft with non-uniform cross-section

Wei *et al. Chin. J. Mech. Eng.*   (2019) 32:70

Page 3 of 13

$\mathbf{y} = [w \quad \phi \quad M \quad Q]^{\mathrm{T}} e^{j\omega t}$, in which, $\mathrm{j} = \sqrt{-1}$, ω is the angular frequency of the elastic waves, the item $e^{j\omega t}$ is usually omitted for it occurs on both sides of the equation. w, ϕ, M, Q are the deflection, slope, moment and shear, respectively [20].

Suppose that the elastic wave propagates from location x_l to location x_r, and then, the motion statuses for locations x_l and x_r can be represented by state vectors $\mathbf{y}_l$ and $\mathbf{y}_r$ respectively. Usually, the propagating process could be indicated by the following equation [20]:

$$\mathbf{y}_r = \mathbf{T}\mathbf{y}_l, \tag{1}$$

where $\mathbf{T}$ is the transfer matrix for the elastic wave.

The propagation characteristics of the elastic waves propagating in the rotating shaft are contained in the transfer matrixes, and which can be obtained by calculating the eigenvalues of the transfer matrix [20]. Set the eigen values of matrix $\mathbf{T}$ to be λ, and which could be expressed as follows

$$\lambda = e^{\mu} = e^{\alpha + j\beta}, \tag{2}$$

where the parameter μ indicates the propagating characteristics, α is named as the attenuation factor, which could indicate the attenuation of the amplitude of the wave components, and β is the phase angel, which indicates the phase gap between the wave components. Eq. (1) could be written in a more obvious way, that is: $(\mathbf{y}_r) = e^{\alpha}(\mathbf{y}_l)e^{\beta}$. It could be deduced that if $\beta = 0$ or $\pm\pi$, the corresponding wave components can't pass through the shaft for the wave components backwards and forwards meeting with each other, and the bands are called as Stop Bands and other bands in which the wave components can pass through are called as Pass Bands [20]. Thus, the transfer matrix should be deduced before studying to the propagation characteristics.

2.2 Additional Equation for an Axial Load

The transfer matrix for the elastic waves in a non-uniform shaft should be derived firstly, and then the analysis to the propagation characteristics can be performed. Often, the transfer matrix can be deduced from the motion equations or the Hamilton's Principle, however, it's difficult to deduce the transfer matrix for a shaft suffering an axial load directly. This paper divides the transfer matrix into two parts, the first part is the transfer matrix $\mathbf{T}_0$ without any axial loads and the second part is the additional transfer matrix $\mathbf{T}_0'$ caused by the axial load.

For a non-uniform shaft without suffering axial loads, former researches have performed detailed study and gained plenty of results, the transfer matrix for the elastic waves is [20, 31]

$$\mathbf{T}_0 = \mathbf{G}(L)e^{\int_0^L \mathbf{H}(x)\mathrm{d}x}\mathbf{G}(0)^{-1}, \tag{3}$$
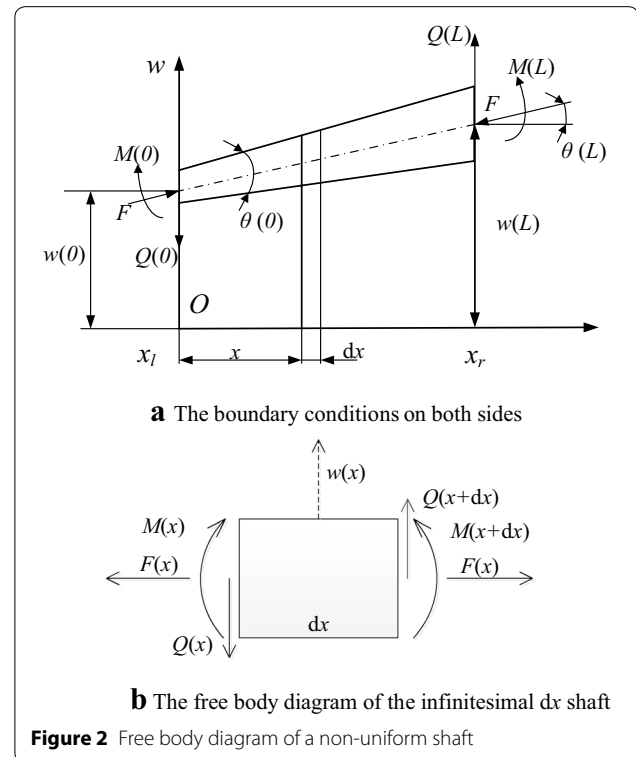
where

$$\mathbf{G}(x) = \begin{bmatrix} 1 & 0 & 0 & 0 \\ 0 & 1 & 0 & 0 \\ 0 & 0 & EI(x) & 0 \\ 0 & 0 & 0 & -EI(x) \end{bmatrix},$$

$$\mathbf{H}(x) = \begin{bmatrix} 0 & 1 & 0 & 0 \\ 0 & 0 & 0 & 1 \\ 0 & 0 & 0 & 1 \\ \frac{\rho S(x)(\omega^2 + \Omega^2) - j\omega\rho I(x)\Omega}{EI(x)} & 0 & -\frac{I_{xx}}{I} & -\frac{2I_x}{I} \end{bmatrix},$$

where Ω is the rotating speed of the shaft, $I(x)$ is the polar moment of the cross-section area at location x. The subscript $(_x)$ indicates the partial derivative to x. And here, I_x and I_{xx} indicate the first and second order partial derivative to x, respectively. The axial load is not considered in Eq. (3).

Next, the paper will focus on deducing the additional equations caused by the axial loads, trying to find out the relationship between the $\mathbf{y}_l$ and $\mathbf{y}_r$ with considering the axial force. As shown in Figure 2, a non-uniform shaft is suffering an axial force F, the free body diagrams for the whole shaft and the infinitesimal length $\mathrm{d}x$ at location x is given out and set $x_l = 0$ and $x_r = L$. Suppose that all the elements on the perpendicular cross-section have the same motion statuses.

a The boundary conditions on both sides

b The free body diagram of the infinitesimal $\mathrm{d}x$ shaft

Figure 2 Free body diagram of a non-uniform shaft

Wei *et al. Chin. J. Mech. Eng.* (2019) 32:70

Page 4 of 13

As shown in Figure 2, The force $F(x)$ is studied as an axial load here, for loads of other type, similar analysis can be adopted too. Since the shaft is in equilibrium, then the Equilibrium Equations can be applied:

$$\begin{cases} \sum F = 0, \\ \sum M = 0. \end{cases} \tag{4}$$

For the left cross-section in Figure 2(a), it can be deduced that

$$F \sin \theta(0) + Q(L) = 0. \tag{5}$$

And similarly, it can be deduced also for the right cross-section, that is

$$F \sin \theta(L) + Q(0) = 0. \tag{6}$$

From Eqs. (5) and (6), we have,

$$Q(L) - Q(0) = F(\theta(L) - \theta(0)). \tag{7}$$

For the cross-section at location x shown in Figure 2(a), the moment here can be written as

$$M(x) = M(0) - Q(0)x. \tag{8}$$

According to the relationship between slope, deflection and moment, that is $M = EI\theta_{,x} = EIw_{,xx}$, and assuming that the deformation is very small, thus, the following equations can be obtained by integrating Eq. (8):

$$\theta(x) = \int \frac{M(0) - Q(0)x}{EI(x)} \mathrm{d}x + \theta(0). \tag{9}$$

Integrate Eq. (9), it can be deduce that

$$w(x) = \iint \frac{M(0) - Q(0)x}{EI(x)} \mathrm{d}x\mathrm{d}x + \theta(0)x + w(0). \tag{10}$$

The relationship between the left section and the right section is needed, thus, substituting $x = L$ into Eqs. (8)–(10), and then

$$M(L) = M(0) - Q(0)L, \tag{11}$$

$$\theta(L) = \int \frac{M(0) - Q(0)x}{EI(x)} \mathrm{d}x + \theta(0), \tag{12}$$

$$w(L) = \iint \frac{M(0) - Q(0)x}{EI(x)} \mathrm{d}x\mathrm{d}x + \theta(0)x + w(0). \tag{13}$$

For the infinitesimal shaft $\mathrm{d}x$ at location x, it can be deduced that

$$Q(x + \mathrm{d}x) - Q(x) = F[\theta(x + \mathrm{d}x) - \theta(x)]. \tag{14}$$

For the whole shaft, Eq. (14) can be rewritten as

$$Q(x) - Q(0) = F[\theta(x) - \theta(0)]. \tag{15}$$

Integrating Eq. (15) from 0 to L and substituting θ with Eq. (12), it can be deduced that the shear force on both ends having the following relationship

$$Q(L) - Q(0) = F \int_0^L \frac{M(0) - Q(0)x}{EI(x)} \mathrm{d}x. \tag{16}$$

From Eqs. (11)–(13) and Eq. (16), the relations between $\mathbf{y}_l$ and $\mathbf{y}_r$ can then be deduced, that is

$$\begin{bmatrix} w \\ \theta \\ M \\ Q \end{bmatrix}_{x_r} = \begin{bmatrix} 1 & L & \int_0^L \int \frac{1}{EI(x)} \mathrm{d}x\mathrm{d}x & \int_0^L \int \frac{x}{EI(x)} \mathrm{d}x\mathrm{d}x \\ 0 & 1 & \int_0^L \frac{1}{EI(x)} \mathrm{d}x & \int_0^L \frac{x}{EI(x)} \mathrm{d}x \\ 0 & 0 & 1 & -L \\ 0 & 0 & \int_0^L \frac{F}{EI(x)} \mathrm{d}x & 1 - \int_0^L \frac{Fx}{EI(x)} \mathrm{d}x \end{bmatrix} \begin{bmatrix} w \\ \theta \\ M \\ Q \end{bmatrix}_{x_l}. \tag{17}$$

As shown in Eq. (17), the axial force only have an influence to the shear and the moment of the state vector, and other parameters are not affected by the axial load $F(x)$. By separating the others and leaving the axial-load-item only, Eq. (17) can be rewritten as

$$\begin{bmatrix} 0 \\ 0 \\ M \\ Q \end{bmatrix}_{x_r} = \begin{bmatrix} 0 & 0 & 0 & 0 \\ 0 & 0 & 0 & 0 \\ 0 & 0 & 0 & 0 \\ 0 & 0 & \int_0^L \frac{F}{EI(x)} \mathrm{d}x & -\int_0^L \frac{Fx}{EI(x)} \mathrm{d}x \end{bmatrix} \begin{bmatrix} 0 \\ 0 \\ M \\ Q \end{bmatrix}_{x_l}. \tag{18}$$

From Eq. (18), it can be obtained that

$$\mathbf{T}'_0 = \begin{bmatrix} 0 & 0 & 0 & 0 \\ 0 & 0 & 0 & 0 \\ 0 & 0 & 0 & 0 \\ 0 & 0 & \int_0^L \frac{F}{EI(x)} \mathrm{d}x & -\int_0^L \frac{Fx}{EI(x)} \mathrm{d}x \end{bmatrix}. \tag{19}$$

Eq. (19) is the additional equation for the axial load to the transfer matrix. The axial load only affects the shear of the state vector.

2.3 Transfer Matrix for the Shaft

Now the transfer matrix for the non-uniform shaft suffering axial loads can then be deduced by combining the additional equation to the transfer matrix deduced without the axial loads.

The additional equation of the axial force has been derived above, see Eq. (18). Considering that the shaft is linear, and then the addition method can be adopted here. Adding Eq. (18) to $\mathbf{y}_r = \mathbf{T}_0 \, \mathbf{y}_l$, and then the transfer matrix for the elastic wave propagating in a non-uniform shaft suffering a axial force load is derived

$$\mathbf{T} = \mathbf{T}_0 + \mathbf{T}'_0, \tag{20}$$

where $\mathbf{T}_0$ and $\mathbf{T}_0'$ have been given out in Eq. (3) and Eq. (19) respectively.

Wei *et al. Chin. J. Mech. Eng.*   (2019) 32:70

Page 5 of 13

Table 1 Geometrical dimensions of the non-uniform rotating shafts

No.	$S(x)$	φ_0 (mm)	$S(0)/S(L)$
1	$S(0)$	30.00	1/1
2	$S(0)(1+x/L)$	30.00	1/2
3	$S(0)(1+2x/L)$	30.00	1/3
4	$S(0)(1+3x/L)$	30.00	1/4

Table 2 The detailed setup for the numerical simulation

	Axial force (N)	Rotating speed (r/min)	Shaft No.
Part 1	0, 100, 200, 300, 400	3000	4
Part 2	400	3000	1, 2, 3, 4
Part 3	400	0, 1500, 3000, 4500	4

According to the definition of the propagation characteristics, they can then be obtained by calculating the eigenvalues of Eq. (20). Here, Eq. (20) is an exponential matrix, and the eigenvalues of which can't be calculated analytically.

3 Numerical Simulation

The transfer matrix of the elastic wave propagating in a non-uniform shaft suffering axial load has been derived in the previous subsection. As mentioned before that the eigenvalues of Eq. (20) can't be solved analytically, a numerical simulation will be adopted here. Noticing that the transfer matrix is associated with the axial load, the rotating speed and the cross-section area variation form, the numerical simulation is then divided into three parts: the first part is to study the influence of the axial force, the second part is to study the influence of the area ratio with considering the axial force, and the last part is to study the influence of the rotating speed of the shaft suffering an axial force.

All the shaft used in this paper are listed in Table 1. Set the locations $x_l = 0$ and $x_r = L$ for the shaft shown in Figure 1, the diameters φ_0 of all the shafts at the location x_l are the same, which are set to be 30.00 mm. The shaft with the cross-section area variation form $S(x) = S(0)(1+3x/L)$ is chosen when studying the influence of the axial load, and the axial loads F is set to be a tension and the value is set to be 0 N, 100 N, 200 N, 300 N, 400 N separately. For the cases of compressions, similar analysis can be adopted too. The area ratio $S(0)/S(L)$ of the shaft is set to be 1/1, 1/2, 1/3 and 1/4, with an axial force 400 N and a rotating speed 3000 r/min. In the last part, the No. 4 shaft is chosen and the rotating speed is set to be 0, 1500 r/min,

3000 r/min, 4500 r/min with axial force 400 N. The detailed information is listed in Table 2.

As shown in Table 1, the lengths of all the shafts are $L = 0.7$ m, with diameter $\varphi_0 = 30.00$ mm at $x = 0$ shown in Figure 1. Supposing the shaft is made of 45# steel, thus, the density ρ is 7.8×10^3 kg/m^3, the elastic modulus E is 2.06×10^{11} Pa and the Poisson's ratio γ is 0.3.

## 3.1 Simulation for Axial Loads

When studying the influence of the axial loads, the axial loads are set to be tensions and the values are 0 N, 100 N, 200 N, 300 N and 400 N, as listed in Table 2. The rotating speed of the shaft to be $\Omega = 3000$ r/min to avoid possible influence caused by the rotating speed fluctuation. Substituting all the parameters into Eq. (20), the eigenvalues and the propagation characteristics of the elastic waves can then be derived by programing in the MATLAB Software. The results are shown in Figure 3.

The Stop Bands derived at different axial loads are shown in Figure 3. The real line and the dashed line are a pair of conjugate values. As can be seen in Figure 3(a), the Stop Bands are [90, 160], [510, 760], [1300, 1670] when F is zero, and the phase angles in the Stop Bands are zero or $\pm\pi$. A new Stop Band [1670, 1780] appears when F increases to 100 N, which is indicated by another real line shown in the figure. The new Stop Band becomes [1430, 1550], [1300, 1425], [1215, 1335] separately when F increased to 200 N, 300 N, 400 N. The original Stop Bands are not signed in the figure for clarity. As for the whole Stop Bands, they can be easily obtained by combining the new Stop Band and the original ones (the Stop Bands derived with F equalling zero). The combined Stop Bands for different axial loads are listed in Table 3.

It can be found in Table 3 that the width of the new Stop Band keeps the same as the increase of the axial load while the central frequency of which decreases gradually. As for the whole Stop Band, only the 3rd one changes while the first two Stop Bands remain the same. A conclusion can be made that the axial load will cause a new Stop Band, and the new Stop Band happens to locate at the range of the third Stop Band, thus, only the 3rd Stop Band is affected by the axial load.

3.2 Simulation for Area Ratios

As shown in Table 2, the shafts numbered 1, 2, 3 and 4 are used to study the influence of the area ratio, the axial force is set to be 400 N and the rotating speed is set to be 3000 r/min to avoid possible influence. Substituting the corresponding parameters into Eq. (20), the propagation characteristics of the elastic waves can then be derived by the same manner mentioned in last subsection. The numerical results are shown in Figure 4.
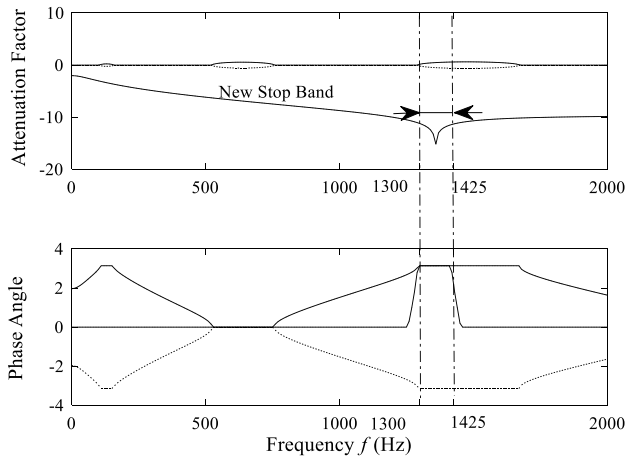
Wei *et al. Chin. J. Mech. Eng.* (2019) 32:70

Page 6 of 13
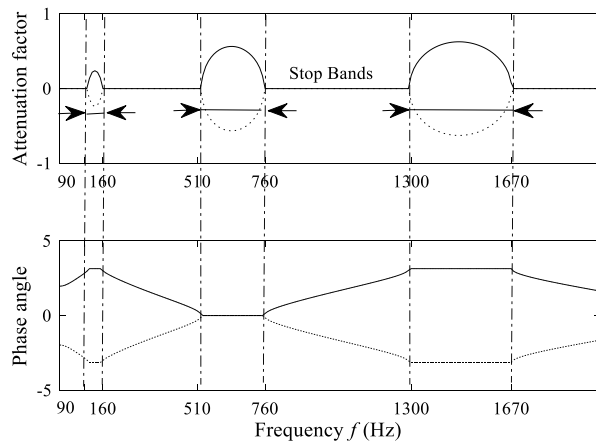
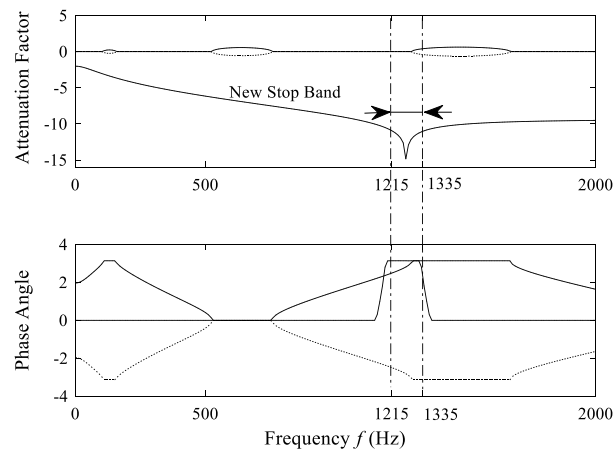**a** Numerical Stop Bands for the case *F*=0 N
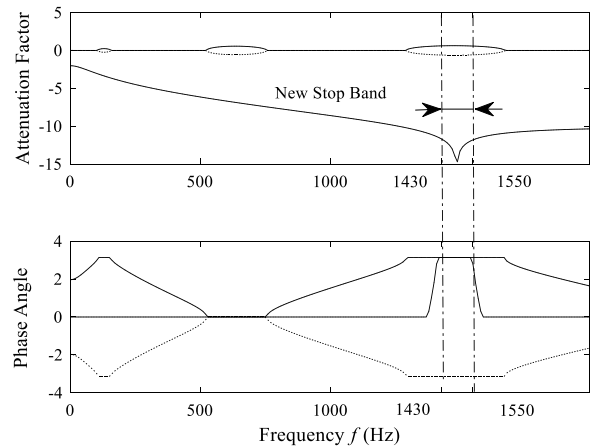
c Numerical Stop Bands for the case *F*=200 N
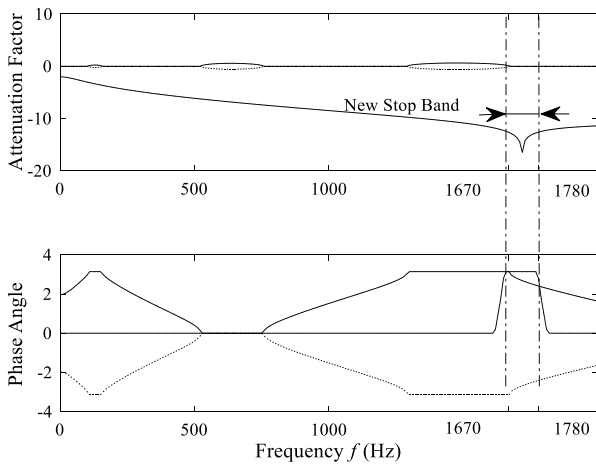
b Numerical Stop Bands for the case *F*=100 N

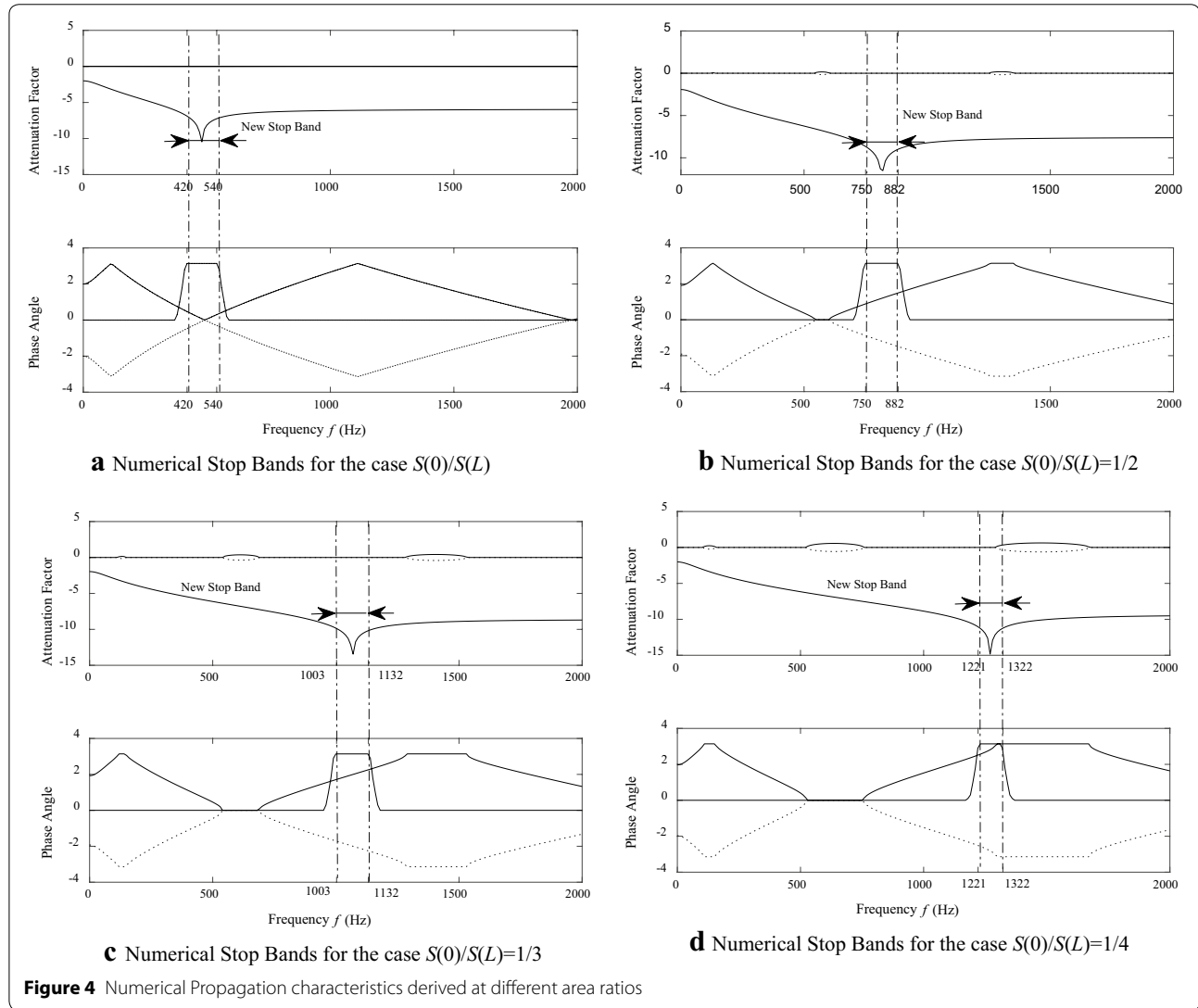**d** Numerical Stop Bands for the case *F*=300 N

e Numerical Stop Bands for the case *F*=400 N

Figure 3 Numerical Stop Bands deduced at different axial forces

Wei *et al. Chin. J. Mech. Eng.*   (2019) 32:70

Page 7 of 13

Table 3 The Stop Bands of Numerical Simulation with different axial forces

Axial Force *F* (N)	New Stop Band	Original Stop Bands (Hz)	Stop Bands (Hz)
0	–	[90, 160] [510, 760] [1300, 1670]	[90, 160] [510, 760] [1300, 1670]
100	[1670, 1780]		[90, 160] [510, 760] [1300, 1780]
200	[1430, 1550]		[90, 160] [510, 760] [1300, 1670]
300	[1300, 1425]		[90, 160] [510, 760] [1300, 1670]
400	[1220, 1320]		[90, 160] [510, 760] [1215, 1670]

a Numerical Stop Bands for the case *S*(0)/*S*(*L*)

b Numerical Stop Bands for the case *S*(0)/*S*(*L*)=1/2

c Numerical Stop Bands for the case *S*(0)/*S*(*L*)=1/3

d Numerical Stop Bands for the case *S*(0)/*S*(*L*)=1/4

Figure 4 Numerical Propagation characteristics derived at different area ratios
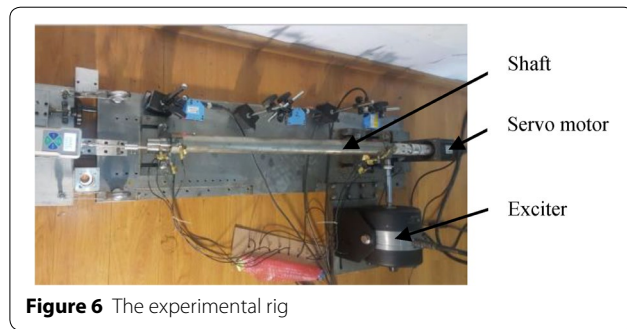
As shown in Figure 4, the new Stop Band is [420, 540] when the area ratio is 1/1 while the original Stop Bands don't show up, and the new Stop Band becomes [750, 882] when the area ratio is 1/2 and the original Stop Bands show up. The new Stop Band are [1003, 1132], [1221, 1322] for the case 1/3 and 1/4 separately. All of the

Stop Bands are listed in Table 4 for easy comparison. The new Stop Band overlaps with the 3rd original Stop Band for the case 1/4.

As can be seen in Table 4, the central frequency of the new emerging Stop Band caused by the axial force will be higher and higher as the increase of the area ratio while

Wei *et al. Chin. J. Mech. Eng.*   (2019) 32:70

Page 8 of 13

Table 4 Numerical Stop Bands derived from different area ratios

Area ratio	New Stop Band (Hz)	Original Stop Bands (Hz)	Stop Bands (Hz)
1/1	[420, 540]	–	[420, 540]
1/2	[750, 882]	[120, 140] [540, 610] [1250, 1350]	[120, 140] [540, 610] [750, 882] [1250, 1350]
1/3	[1003, 1132]	[110, 150] [530, 700] [1280, 1540]	[110, 150] [530, 700] [1003, 1132] [1280, 1540]
1/4	[1221, 1322]	[105, 160] [520, 760] [1290, 1675]	[105, 160] [520, 760] [1221, 1675]
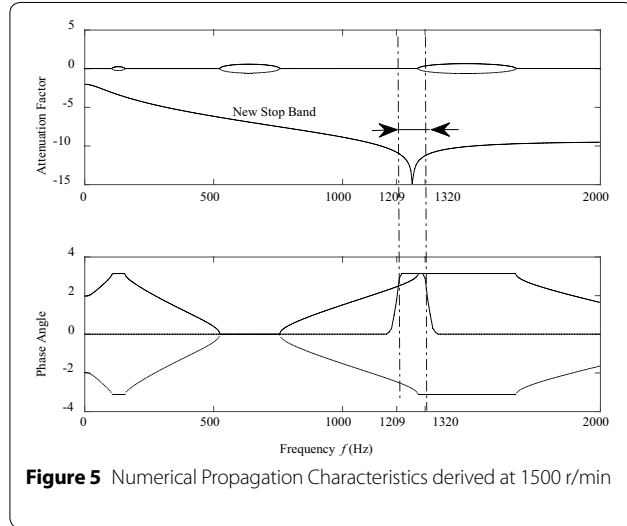
Figure 5 Numerical Propagation Characteristics derived at 1500 r/min

Figure 7 Mechanism for applying axial force

Figure 6 The experimental rig
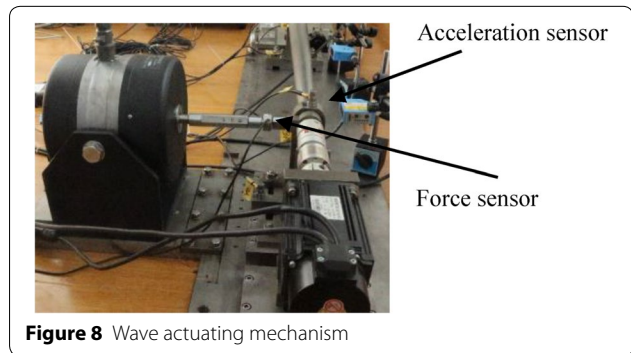
Figure 8 Wave actuating mechanism

the width of which remains the same, and the widths of the original Stop Bands become larger and larger as the increase of the area ratio too.

3.3 Simulation for Rotating Speeds

When studying the influence of the rotating speed, the shaft with area ratio $S(0)/S(L) = 1/4$ is chosen, and the axial load F is set to be a constant value 400 N. Substituting the corresponding parameters into Eq. (20), the propagation characteristics of the elastic waves can then be derived by calculating the eigenvalues of the transfer matrix. The numerical results are shown in Figure 5.

The numerical propagation characteristics derived at different rotating speed varies slightly. The results derived at 1500 r/min is taken as an example here. It can be found that the new Stop Band is [1209, 1320] and the three original Stop Bands are [105, 154], [523, 756], [1301, 1672]. The new Stop Band overlaps with the 3rd Stop Band. The Stop Bands are [105, 154], [523, 756], [1209, 1672] by merging the new Stop Band and the three original Stop Bands.

4 Experimental Analysis

An experimental rig is setup and the experiments are performed according to the procedures of the numerical simulation. The rig is shown in Figure 6. The shaft to be tested is supported by two sliding bearings which are fixed on a steel base, and the shaft is driven by a servo

motor which can control the rotating speed of the shaft precisely. A set of acceleration sensors are fixed on the bearings and on the steel base.

The axial load is exerted by a pull rod which is connected to a digital tension gauge, see Figure 7. A signal function generator generates a pulse signal, and then the signal is amplified by an amplifier and sent to the exciter, and then the exciter acts a force on the shaft which is used to stimulate the elastic wave, just shown as Figure 8. The acceleration sensors are set on the two sliding bearings and the acceleration signals of both sides are acquired by a date acquiring system.

A single or a set of pulse is often used to stimulate the elastic wave [20, 32], a single pulse is used in this paper. The signal generator generates a pulse with a width of 2×10^{-3} s and then the pulse is amplified by an amplifier, the amplified signal is then used to drive the exciter. The force of the exciter acting on the shaft is measured by a force sensor, as shown in Figure 8. The magnitude of the force is limited to 100 N to avoid overloads for the sensors.

In order to verify the results of the numerical simulation, the experiments are performed as the numerical simulation. The experiments are performed to validate the influence of the axial load, the area ratio and the rotating speed, following the conditions shown in Table 2. Besides the non-uniform shafts, the uniform shafts with the same mass are studied too. The diameters of the uniform shafts are 30.00 mm, 36.74 mm, 42.43 mm, 47.43 mm for the non-uniform shafts numbered 1, 2, 3 and 4 separately.

4.1 Experimental Results for Axial Force

The actuating force is used to stimulate the elastic force and be studied firstly. The time history of the real stimulating force and its spectrum obtained by the FFT (Fast Fourier Transformation) are shown in Figure 9.

As can be seen in Figure 9, the energy of the signal mainly distributes at the range [0, 2000], which covers the width of the numerical simulation, thus the force can be

used to study the propagation characteristics of the elastic waves.

Alternative magnitudes of the axial force are studied and the result are shown in Figure 10. Acceleration signals of the non-uniform shaft and the uniform shaft with the same mass are studied. Considered the complexity of the signals, the spectrum comparison method is used here to determine the Stop Bands of the elastic waves. A very short signals of 0.02 s' length after the stimulating force is obtained by truncating the original ones. Considering that the difference of the numerical Stop Bands lies at the third Stop Band, the comparison focuses on the 3rd Stop Band here.

As can be seen from Figure 10, the length of the time history is 0.02 s, the dashed lines indicate time- and frequency-domain of the signal for the non-uniform shaft, while the real lines indicate those for the uniform shaft processing the same volume. In Figure 10(a), the spectrum in the range [1250, 1680] for the uniform shaft is higher than that that for the non-uniform shaft, thus, this range is a Stop Band for the case $F = 0$. Similarly, the Stop Bands are [1305, 1795], [1292, 1690], [1271, 1752] for the axial forces 100 N, 200 N, 300 N, 400 N separately. The Stop Bands match well with the numerical ones, which indicates the validation of the theoretical result. The axial load will cause a new Stop Band's appearance, and the central frequency of which will decrease as the increase of the force while the width remains the same.
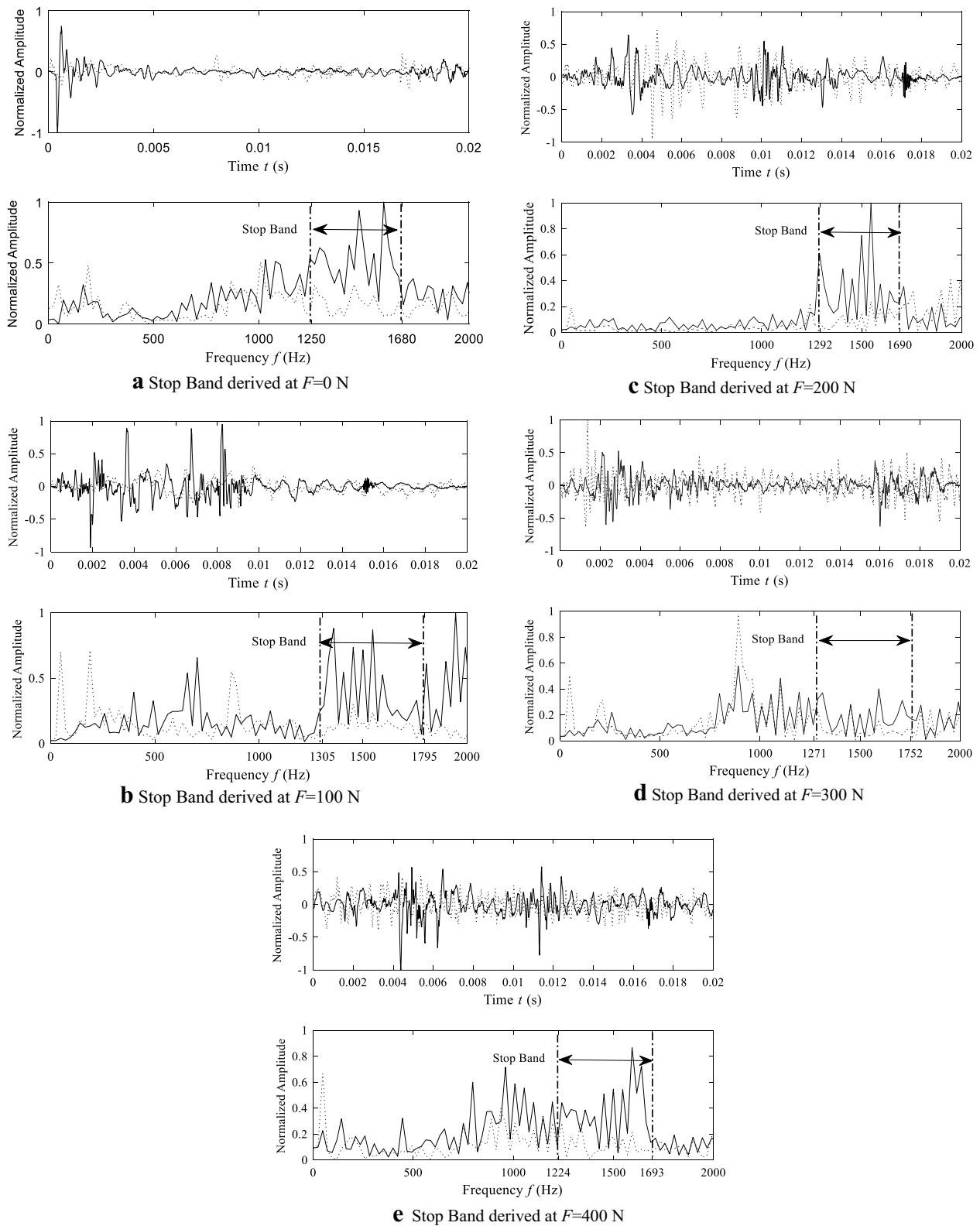
4.2 Experimental Results for Area Ratio

As shown in Table 2, the shafts Numbered 1, 2, 3, 4 are used in the experiments too. In order to isolate other factor's influence, the axial force is chosen as 400 N, and the rotating speed is set as 3000 r/min. The experiment results are shown in the following figure.
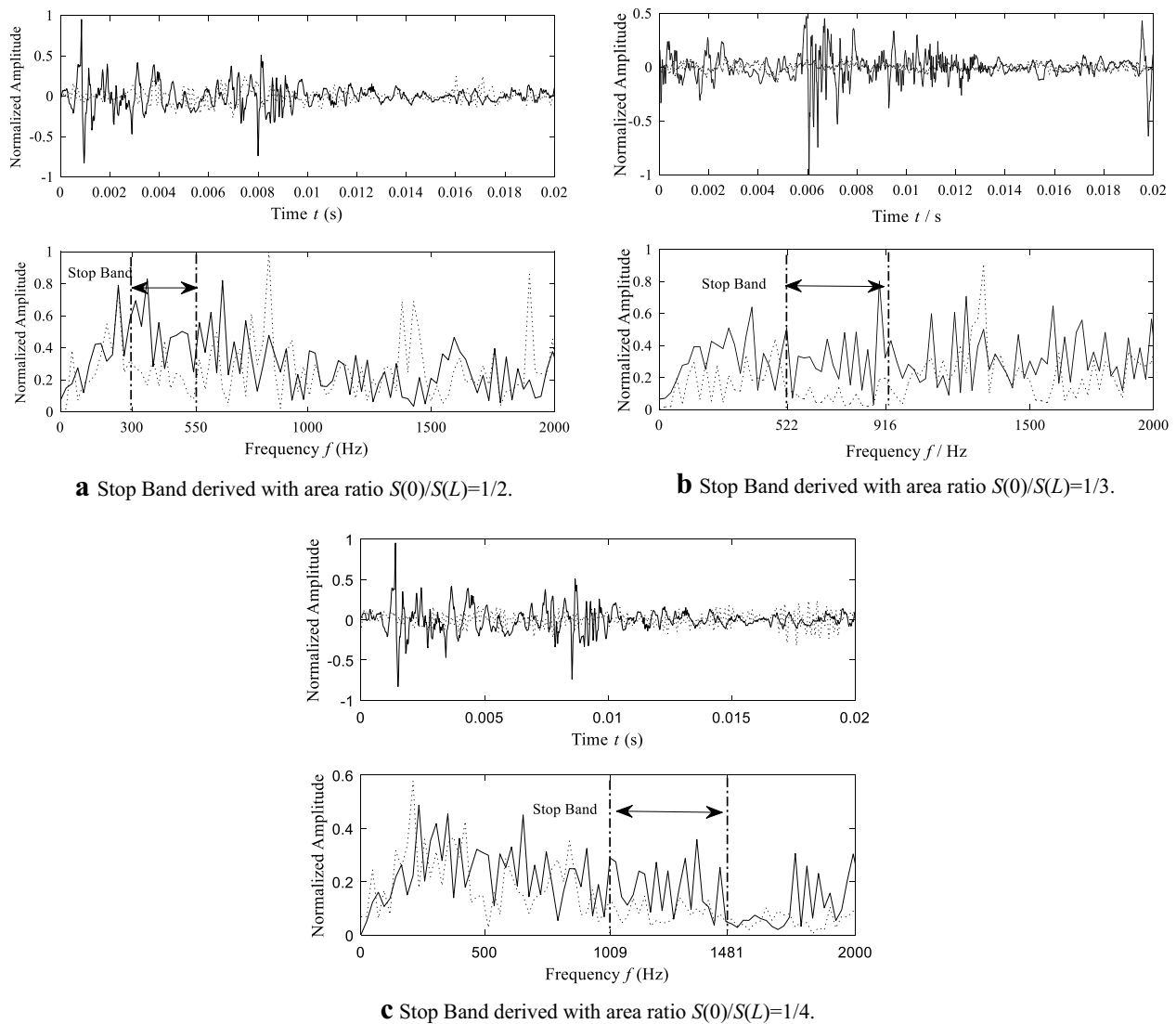
It can be seen from Figure 11 that the Stop Band is [300, 550] for the case $S(0)/S(L) = 1/2$, and the Stop Bands are [522, 916], [1009, 1481] for the case $S(0)/S(L) = 1/3$ and $S(0)/S(L) = 1/4$ separately. Compared with the numerical Stop Bands listed in Table 4, it can be found that the Stop Band are [120, 140] [540, 610] [750, 882] [1250, 1350] for the case $S(0)/S(L) = 1/2$, while the Stop Bands are [110, 150] [530, 700] [1003, 1132] [1280, 1540] for the case $S(0)/S(L) = 1/3$, and the Stop Bands are [105, 160] [520, 760] [1221, 1675] for the case $S(0)/S(L) = 1/4$. Although there are gaps between the experimental results and the numerical ones. The experiments can also verify the validation of the numerical conclusion that the central frequency of the new Stop Band will increase as the increase of the area ratio while the width of which remains the same,
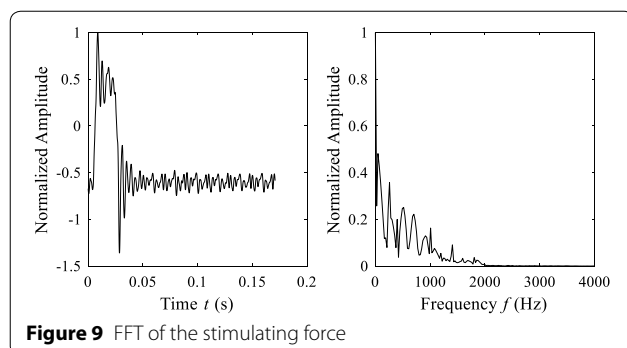
Figure 9 FFT of the stimulating force

Figure 10 Experimental Stop Band derived at different loads

Wei *et al. Chin. J. Mech. Eng.* (2019) 32:70

Page 11 of 13

a Stop Band derived with area ratio $S(0)/S(L)$=1/2.

b Stop Band derived with area ratio $S(0)/S(L)$=1/3.

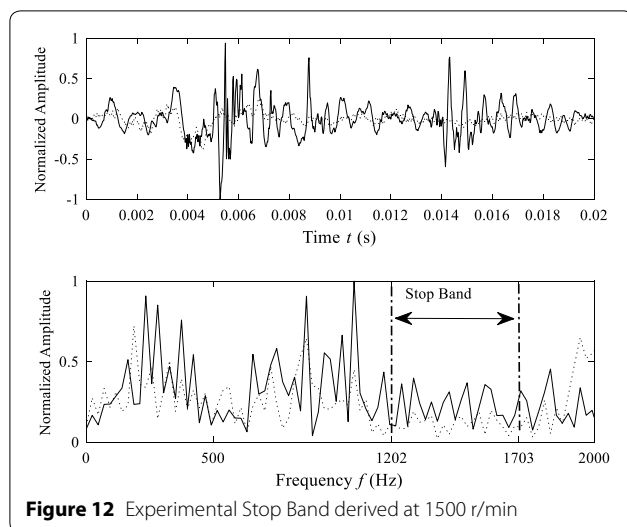**c** Stop Band derived with area ratio $S(0)/S(L)$=1/4.

Figure 11 Experimental Stop Band derived at different area ratios

and the original Stop Bands will be larger and larger as the increase of the area ratio.

4.3 Experimental Results for Rotating Speeds
A set of rotating speeds of the shafts are adopted here. However, the experimental results are the same at alternative rotating speeds. The experimental result derived at 1500 r/min is used here as an example, which is shown in Figure 12.

It can be seen from the above figure that the Stop Band is [1202, 1703]. The experiment result is in accordance with the numerical one of the theoretical study, though there are gaps between them. The Stop Bands remain the same though the rotating speed changes.

Wei *et al. Chin. J. Mech. Eng.* (2019) 32:70

Page 12 of 13

Figure 12 Experimental Stop Band derived at 1500 r/min

5 Conclusions

(1) The transfer matrix of the elastic waves for the non-uniform shaft with axial loads is deduced by combining the matrix without axial loads and the additional equation caused by the axial load.

(2) A new Stop Band will appear due to the axial load. The width of the new Stop Band remains the same while the central frequency decreases gradually as the increase of the axial load.

(3) The central frequency of the new Stop Band will increase as the increase of the area ratio while the width of which remains the same, and the original Stop Bands will be larger and larger as the increase of the area ratio.

(4) The Stop Bands vary slightly as the change of the rotating speed of the non-uniform shaft.

Authors' Contributions
YW performed the theoretical analysis; ZZ and QL applied the numerical simulation; WC designed the experiments; ZZ carried out the experiments; YW analyzed the data and wrote the manuscript. All authors read and approved the final manuscript.

Authors' Information
Yimin Wei, born in 1986, is currently a teacher at *National and Local Joint Engineering Research Center of Reliability Analysis and Testing for Mechanical and Electrical Products, Zhejiang Sci-Tech University, China*. He received his doctor's degree on Mechanical Engineering from *Zhejiang University*, China, in 2014. His research interests include the dynamics and fault diagnosis and prognostic.

Zhiwei Zhao, born in 1992, is currently an engineer at *Hangzhou Hikvision Digital Technology Co., Ltd, China*. He received his master's degree from *Zhejiang Sci-tech University, China*, in 2018.

Wenhua Chen, born in 1963, is currently the vice-president of *Zhejiang Sci-Tech University, China*. He received his doctor's degree on Mechanical Engineering from *Zhejiang University, China*, in 1997. His research interests include the reliability and the ALT of mechanical and electrical product.

Qi Liu, born in 1990, is currently an engineer at *Hangzhou Hikvision Digital Technology Co., Ltd, China*. He received his master's degree from *Zhejiang Sci-Tech University, China*, in 2018.

References

[1] Y Yang, Y Xu, Y Yang, et al. Dynamics characteristics of a rotor-casing system subjected to axial load and radial rub. *International Journal of Non-Linear Mechanics*, 2018, 99(12): 59-68.

[2] M Takla. Non-symmetric bifurcation and collapse of elastic-plastic thick-walled cylinders under combined radial and axial loading. *Marine Structures*, 2019, 64(1): 246-262.

[3] U J F Aarsnes, N Van De Wouw. Axial and torsional self-excited vibrations of a distributed drill-string. *Journal of Sound and Vibration*, 2019, 444(1): 127-151.

[4] A Bahrami, A Teimourian. Study on vibration, wave reflection and transmission in composite rectangular membranes using wave propagation approach. *MECCANICA*, 2017, 52(1-2): 231-249.

[5] C Gan, Y Wei, S Yang. Longitudinal wave propagation in a multi-step rod with variable cross-section. *Journal of Vibration & Control*, 2016, 22(3): 837-852.

[6] C Gan, Y Wei, S Yang. Longitudinal wave propagation in a rod with variable cross-section. *Journal of Sound and Vibration*, 2014, 333(2): 434-445.

[7] Y Wei, X Shi, Q Liu, et al. The influence of crack modes on the elastic wave propagation characteristics in a non-uniform rotating shaft. *Applied Sciences*, 2018, 8(11): 2105,1-19.

[8] Y Wei, S Yang, W Chen, et al. The influence of transverse cracks to propagation characteristics of elastic waves propagating in a non-uniform shaft. *Journal of Sound and Vibration*, 2019, 444(1): 35-47.

[9] M Zhang, L Xiao, W Qu, et al. Damage detection of fatigue cracks under nonlinear boundary condition using subharmonic resonance. *Ultrasonics*, 2017, 77(1): 152-159.

[10] S Kocakaplan, J L Tassoulas. Wave propagation in initially-stressed elastic rods. *Journal of Sound and Vibration*, 2019, 443(1): 293-309.

[11] M M Ahmadi, S Mahvelati. A new approach for group efficiency of drilled shafts in sand subjected to axial loading. *International Journal of Geotechnical Engineering*, 2016, 1(1): 1-13.

[12] M Eftekhari, A D Rahmatabadi, A Mazidi. Nonlinear vibration of inextensional rotating shaft under electromagnetic load. *Mechanism and Machine Theory*, 2018, 121(1): 42-58.

[13] Y Huang, A Liu, Y Pi, et al. Assessment of lateral dynamic instability of columns under an arbitrary periodic axial load owing to parametric resonance. *Journal of Sound and Vibration*, 2017, 395(1): 272-293.

[14] T Chen, Z Xia, X Wang, et al. Experimental study on grouted connections under static lateral loading with various axial load ratios. *Engineering Structures*, 2018, 176(1): 801-811.

[15] Q Dai, Q Cao. Parametric instability of rotating cylindrical shells subjected to periodic axial loads. *International Journal of Mechanical Sciences*, 2018, 146-147(1): 1-8.

[16] G Gholipour, C Zhang, A A Mousavi. Effects of axial load on nonlinear response of RC columns subjected to lateral impact load: Ship-pier collision. *Engineering Failure Analysis*, 2018, 91(1): 397-418.

[17] A Johansen, G Solland, A Lervik, et al. Testing of jacket pile sleeve grouted connections exposed to variable axial loads. *Marine Structures*, 2018, 58(1): 254-277.

Wei *et al. Chin. J. Mech. Eng.*   (2019) 32:70

Page 13 of 13

[18] Y H Dong, B Zhu, Y Wang, et al. Analytical prediction of the impact response of graphene reinforced spinning cylindrical shells under axial and thermal loads. *Applied Mathematical Modelling*, 2019, 71(1): 331-348.

[19] P Vainshtein. On wave propagation in waveguides. *Physica D: Nonlinear Phenomena*, 2002, 162(1–2): 1-8.

[20] M Toso. *Wave propagation in rods, shells, and rotating shafts with non-uniform geometry*. Maryland: University of Maryland, 2004.

[21] A T Fabro, N S Ferguson, B R Mace. Wave propagation in slowly varying waveguides using a finite element approach. *Journal of Sound and Vibration*, 2019, 442(1): 308-329.

[22] Q S Li. Exact solutions for free longitudinal vibration of stepped non-uniform rods. *Applied Acoustics*, 2000, 60(1): 13-28.

[23] Q S Li. Free longitudinal vibration analysis of multi-step non-uniform bars based on piecewise analytical solutions. *Engineering Structures*, 2000, 22(9): 1205-1215.

[24] S Abarbanel, A Ditkowski. Wave propagation in advected acoustics within a non-uniform medium under the effect of gravity. *Applied Numerical Mathematics*, 2015, 93(1): 61-68.

[25] A Bahrami, A Teimourian. Study on the effect of small scale on the wave reflection in carbon nanotubes using nonlocal Timoshenko beam theory and wave propagation approach. *Composites Part B: Engineering*, 2016, 91(1): 492-504.

[26] K Xie, M Chen, L Zhang, et al. Free and forced vibration analysis of non-uniformly supported cylindrical shells through wave based method. *International Journal of Mechanical Sciences*, 2017, 128-129(1): 512-526.

[27] O Tavasoli, M Ghazavi. Wave propagation and ground vibrations due to non-uniform cross-sections piles driving. *Computers and Geotechnics*, 2018, 104(1): 13-21.

[28] X Xue, X Chen, X Zhang, et al. Hermitian plane wavelet finite element method: Wave propagation and load identification. *Computers & Mathematics with Applications*, 2016, 72(12): 2920-2942.

[29] S M Mousavi Janbeh Sarayi, A Bahrami, M N Bahrami. Free vibration and wave power reflection in Mindlin rectangular plates via exact wave propagation approach. *Composites Part B: Engineering*, 2018, 144(1): 195-205.

[30] A Bahrami, A Teimourian. Free vibration analysis of composite, circular annular membranes using wave propagation approach. *Applied Mathematical Modelling*, 2015, 39(16): 4781-4796.

[31] Y Wei. *Equations of motion and propagation characteristics of elastic waves propagating in rods and rotating shafts with variable cross-section*. Hangzhou: Zhejiang University, 2014. (in Chinese)

[32] A Żak, M Krawczuk. Certain numerical issues of wave propagation modelling in rods by the Spectral Finite Element Method. *Finite Elements in Analysis and Design*, 2011, 47(9): 1036-1046.